

Structure changes in mono-crystalline silicon subjected to indentation — experimental findings

I. Zarudi, L.C. Zhang *

Department of Mechanical and Mechatronic Engineering, The University of Sydney, NSW 2006, Australia

Received 2 May 1999; received in revised form 10 September 1999; accepted 14 December 1999

Abstract

This paper investigates the subsurface deformation in silicon induced by indentation. With the precise cross-sectioning technique and high-resolution electron microscopy, a number of new phenomena were discovered. These include the phase transformation to amorphous, bcc and tetragonal silicon, the emergence of planar defects and the onset of microcracking. The study drew a relatively complete picture of silicon deformation under a range of indentation conditions. © 2000 Elsevier Science Ltd. All rights reserved.

Keywords: Silicon; Indentation; High-resolution; Phase transformation; Planar defects

1. Introduction

The indentation of silicon and related micro-structural changes have been the focus of research over the last 10 years [1–10]. Most of the researches have addressed mainly the load–displacement behaviour [3–5] and concluded that it was the hydrostatic stress that brought about a tetragonal phase formation during loading followed by a phase transformation to bcc structure upon unloading. The formation of amorphous phase during nano-indentation was also reported [2,9–11]. However, most of these results were not directly confirmed by indentation experiments and the shape and structure of the transformation zone in indentation were not revealed. The only evidence of the existence of the tetragonal phase on loading is through the measurement of conductivity [1,2], although traces of some mottled phase in indentation were admitted [10] and the amorphous phase inside the residual indents was identified by means of transmission electron microscopy [2,10]. It was also reported [11] that under nano-indentation silicon showed little or no dislocation activity but highly disturbed structures.

A recent study by means of the molecular dynamics

analysis provided theoretical evidence for the amorphous phase change in silicon indentation and established a criterion for predicting its formation [7,8]. It was found that if the indentation stress was not high enough to form a metallic phase during loading, amorphous phase transformation upon unloading could not emerge [12]. Repeated indentation does not very much alter the amorphous zone caused by the first indentation [13]. In the relevant studies on ultra-precision machining on the nanometre scale, it was also reported that amorphous phase transformation is indeed the major residual deformation in ground and polished specimens but dislocations may also appear in certain circumstances [14,15].

Although there existed some investigations using transmission electron microscope to study the indented silicon specimens, the analysis was based on plan-view examinations [2,10]. This approach has a significant limitation, as subsurface damages caused by indentation cannot be observed in the direction perpendicular to the indented surface, so that the details of micro-structural changes of the material cannot be explored.

The present work aims to analyse the subsurface structure of indented mono-crystalline silicon by means of high-resolution electron microscopy on cross-section view samples, although it is extremely difficult technically, to avoid the disadvantage in existing experiment and to reveal, to the full extent, the micro-structural changes in silicon after indentation.

* Corresponding author. Tel.: +61-2-9351-2835; fax: +61-2-9351-3760.

E-mail address: zhang@mech.eng.usyd.edu.au (L.C. Zhang).

2. Experimental procedure

All experiments were conducted on precisely polished (100) surfaces of mono-crystalline silicon with a rms surface roughness of 2 nm. Similar to our previous studies on grinding and polishing [14] the subsurface structure of specimens was examined to guarantee that a specimen was damage-free before indentation.

The load–displacement measurements of indentation with a spherically tipped diamond indenter of radius 5 μm were made on a UMIS-2000 instrument whose details can be found elsewhere [16]. To understand the micro-structural changes with respect to indentation, a series of tests were conducted under total indentation loads of 30, 40, 50, 70, 90 and 100 mN, respectively. In each test, 100 indentation depths were measured throughout the loading–unloading cycle.

To fully explore the deformation of silicon under indentation, it is theoretically necessary to examine the cross-section of a specimen that is just cut through the symmetric axis of indentation, as shown in Fig. 1. However, this is very difficult to achieve experimentally. A residual indentation mark on a specimen is so small, with a characteristic dimension from a fraction of a micron to a few microns depending on the magnitude of the total indentation load, that a special procedure must be used to identify such an indentation mark and to prepare a satisfactory cross-section view sample. To this end, an indentation array, under an identical indentation load, was first generated, as shown in Fig. 2(a). Before cross-sectioning, the characteristic dimension of the indentation marks was measured using an atomic force microscope (AFM) for reference as schematically illustrated

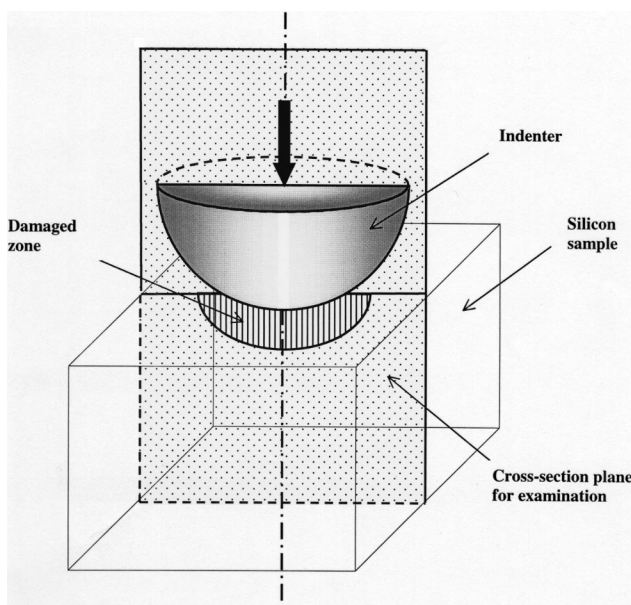


Fig. 1. The cross-section plane for subsurface damage examination of a sample under indentation with a spherical diamond indenter.

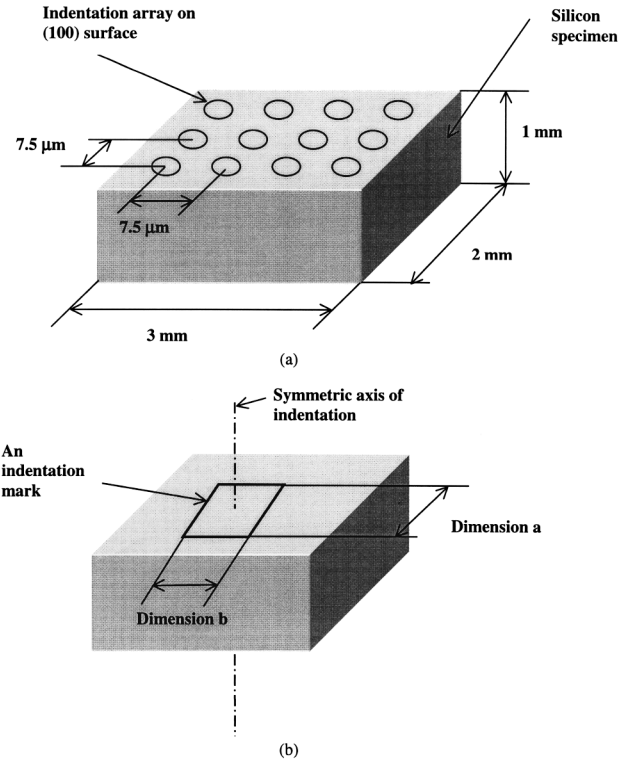


Fig. 2. Details of the preparation of the cross-section view samples. (a) Indentation array; (b) characteristic dimension of the residual indentation marks in AFM; (c) estimation of the cross-sectioning angle; (d) matching of the characteristic dimension after cross-sectioning.

in Fig. 2(b). The cross-section angle α (Fig. 2(c)) was then estimated to ensure that a number of indentation marks would be cut through by the cross-section surface. The sides of the slice cut were first thinned down mechanically under an optical microscope until they were about 1–2 μm from the edges of the indentation marks. Further thinning was then done by an ion-beam thinner (PIPS Model 691) with a concentrated ion-beam from the side opposite to the indented surface to avoid introducing any damage to the indented surface in specimen preparation.

Subsurface structure of the material was then examined by means of a transmission electron microscope (TEM), CM12 and scanning transmission electron microscope (STEM), VG HB601 HREM, with a point spatial resolution of 0.22 nm, operating voltage of 100 kV and electron beam direction along [011] of silicon. During TEM and STEM examination the residual deformation zones were compared with the reference dimensions recorded by AFM (Fig. 2(d)). A good matching in this way guaranteed that the cross-section view was through the axis of indentation to a great extent. However, if none of the residual zones thus obtained matched the AFM references, the above preparation process must be repeated until a satisfactory specimen was produced.

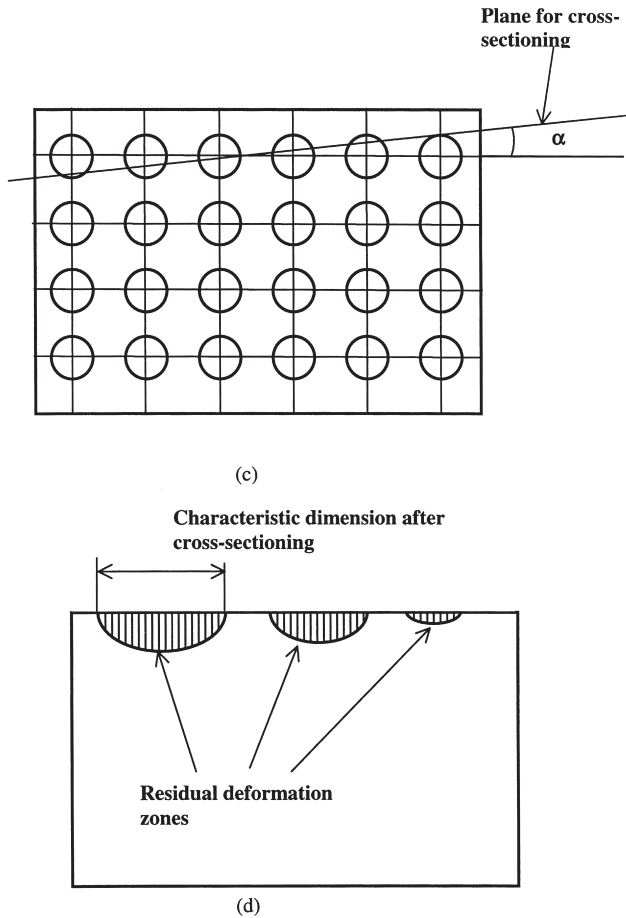


Fig. 2. (continued)

At least five indentation marks were examined after cross-sectioning under each indentation load.

3. Results and discussion

3.1. Residual indentations

Results on the penetration depth of the indenter at different loads and dimensions of the residual indentations are listed in Table 1 and shown in Fig. 3(a). If the defor-

mation is purely elastic, then the theory of indentation mechanics [17] shows that

$$\delta = \left(\frac{9P^2}{16RE^{*2}} \right)^{1/3} \quad (1)$$

with the slope

$$\frac{d\delta}{dP} = \left(\frac{1}{6RE^{*2}} \right)^{1/3} P^{-1/3} \quad (2)$$

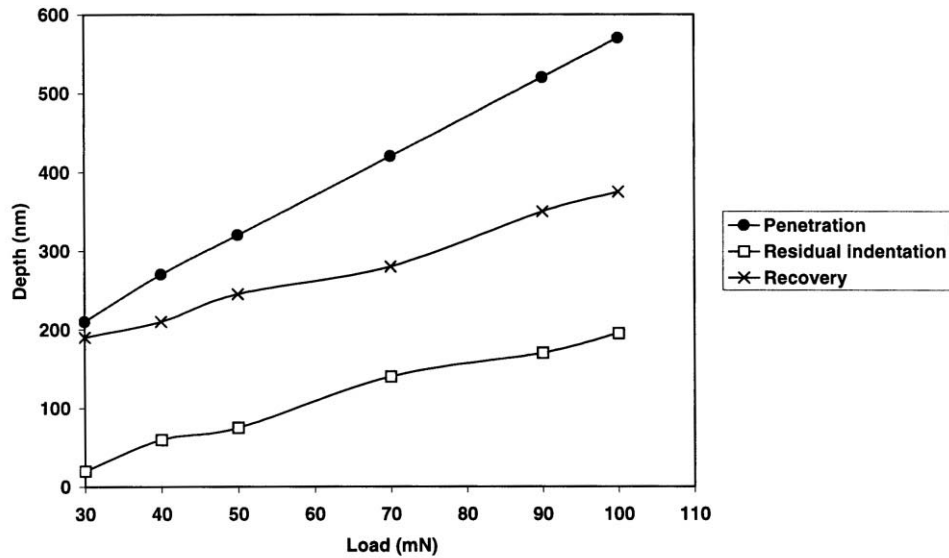
where δ is the penetration depth, P is the indentation load,

$$E^* = \left(\frac{1-\nu_{\text{ind}}^2}{E_{\text{ind}}} + \frac{1-\nu_{\text{si}}^2}{E_{\text{si}}} \right)^{-1} \quad (3)$$

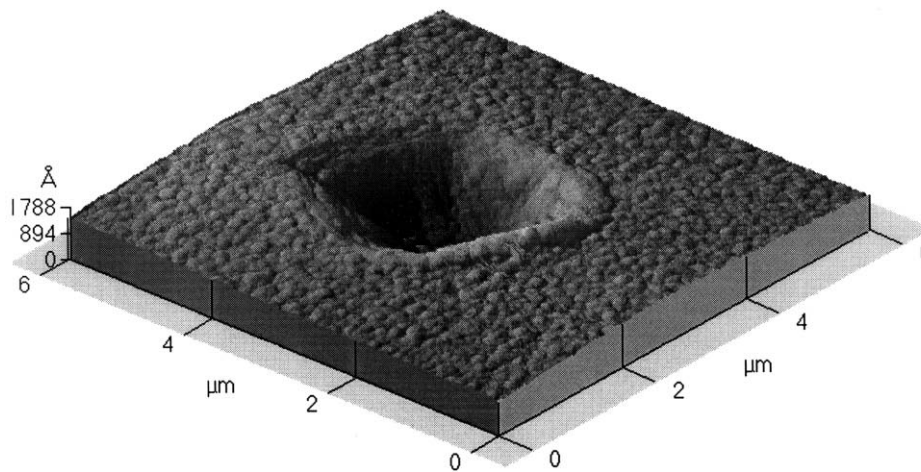
where ν_{ind} and E_{ind} are Poisson's ratio and elastic modulus of the diamond indenter and ν_{si} and E_{si} are Poisson's ratio and elastic modulus of silicon, R is the indenter radius. For silicon, when the indentation load varies from 30 to 100 mN, the slope $d\delta/dP$ changes from 3.6 to 2.5 nm/mN. However, the indentation tests (Fig. 3(a)) showed that the penetration depth increases with a slope varying from 4.8 to 5.2 nm/mN. Such a deviation from the elastic Hertzian behaviour indicates that plastic deformation took place in all the indentation conditions tested. This is well confirmed by the residual indentation marks, as shown in Fig. 3(b), which is a three-dimensional image of a typical residual indentation mark on the (100) surface of silicon. It can be seen clearly that the edge of the mark is non-circular and is with a ratio of characteristic dimensions $b/a=0.8$. This value is in very good agreement with that obtained by molecular dynamic simulation [8] and is dependent on the deformation properties of silicon in different crystallographic directions. However, a deviation of an indenter's profile from a perfect spherical shape can also contribute to the formation of a non-circular indentation mark. To exclude this possibility, additional indentation marks were performed by rotating specimens about the indentation axis while the indenter's orientation was kept unchanged. In this way, if the indenter was non-spherical, the non-circular profiles of the residual indentation marks would orientate in different crystallographic directions of sili-

Table 1
Experimental parameters of the transformation zone at different indentation loads

Indentation load (mN)	Penetration (nm)	Residual indentation (nm)	Width of the transformation zone (μm)	Depth of the transformation zone (nm)	Defect penetration (μm)
30	210	20	0.56	95	0.6
40	270	60	0.96	180	0.9
50	320	75	1.5	270	2.3
70	420	140	1.66	500	2
90	520	170	2.6	700	2.5
100	570	195	2.7	800	2



(a)



(b)

Fig. 3. (a) Effect of indentation load on the penetration depth of indentation, depth of residual indentation mark and recovery; (b) the three-dimensional image of a typical residual indentation mark (indentation load=100 mN).

con. Nevertheless, it was observed that all residual indentation marks were elongated in the same *crystallographic* directions that were independent of the rotation angles of the specimens. This means that the formation of the non-circular marks were due to the anisotropy of the material rather than the shape inaccuracy of the indenter. The comparison of the penetration depth of indenter with the depth of the residual marks indicates that the recovery during unloading has been significant (Fig. 3(a)). There are always some pile-ups around the indentation edge (Fig. 3(b)) caused by extrusion of the ductile phase of silicon during indentation. No cracks were found on the indented surface.

3.2. Subsurface structure after indentation

The subsurface structures of silicon at indentation loads from 30 to 100 mN are shown in Figs. 4–10. The common feature of deformation is the development of the transformation zones in the immediate vicinity of the subsurface region. A typical transformation zone has nearly a hemispherical shape when the indentation load is small (Figs 4(a), 5, 6(a) and 8(a)) and approaches to conical when the load becomes large (Figs 9(a) and 10(a)). The depth of the zone increases nearly proportionally to the indentation load (Table 1 and Fig. 11) which is similar to the variation of the residual inden-

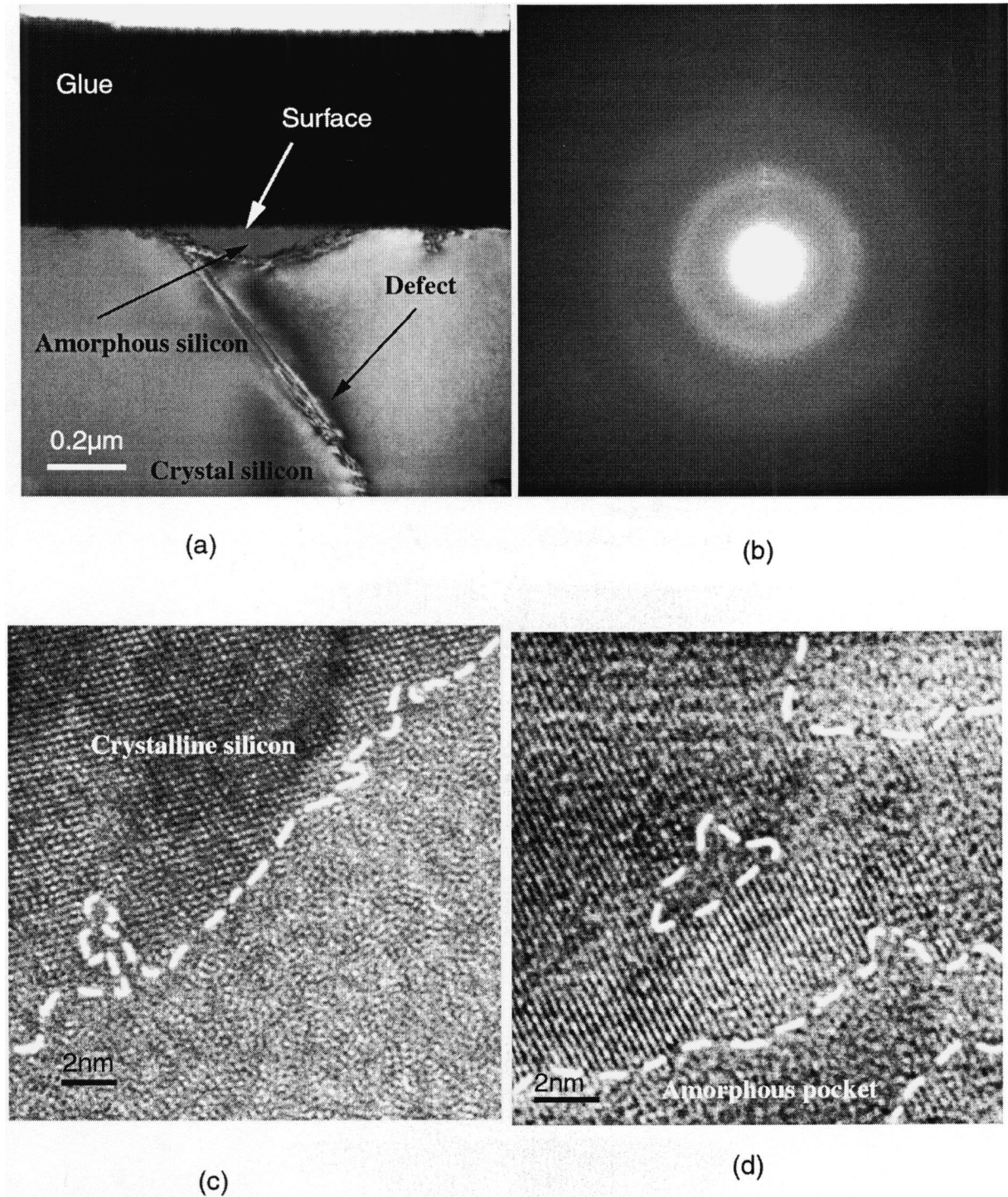


Fig. 4. Subsurface damage at the indentation load of 30 mN. (a) General view of the transformation zone; (b) diffraction pattern of the transformation zone; (c) amorphous-crystalline interface in high-resolution mode (note the roughness of the interface); (d) amorphous pockets at the interface.

tation marks on the sample, as shown in Fig. 4. Theoretical predictions of the depth and width of the amorphous phase, based on the threshold (4.6 GPa along 100 direction in silicon) and the octahedral shearing stress (OSS) criterion developed by Zhang and Tanaka [8,9], are shown in Fig. 11. The theoretical depth of the transformation zone increases linearly with the indentation load

and has the same slope as the experimental curve. Fig. 11 shows that the theoretically predicted depth is always larger than the experimental values. It is reasonable, because the experimental measurement was after unloading during which significant recovery took place, as shown both theoretically [8] and experimentally in Fig. 3(a). However, the width of the transformation zone

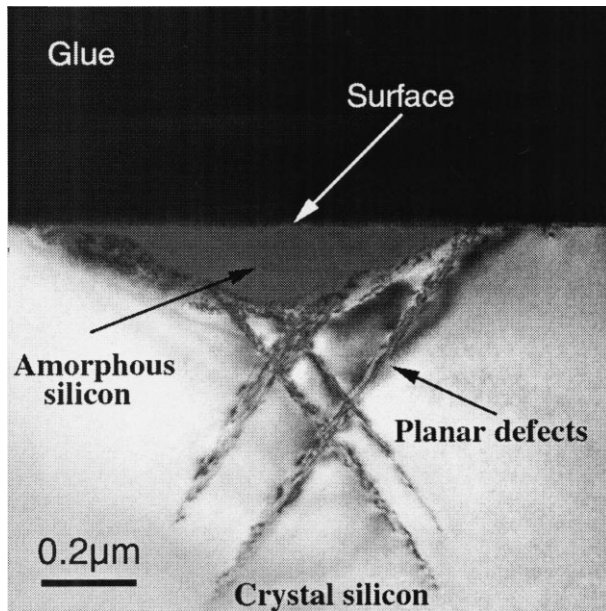
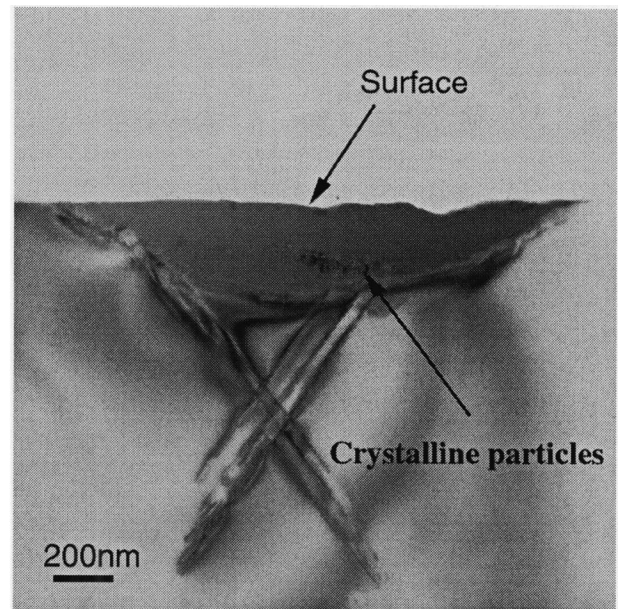


Fig. 5. Subsurface deformation at the indentation load of 40 mN.



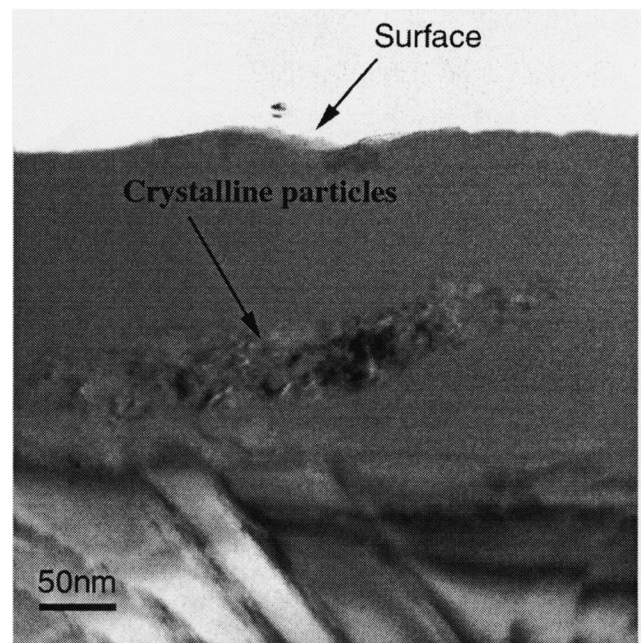
(a)

varies with the load in a more complex manner, as shown in Fig. 11. The difference between theory and experiment is large. Unfortunately the authors cannot explain the deviation so far.

There are always some defects emanating from the bottom of the transformation zone. These defects lie in $\{111\}$ planes and their penetration depth increases with increasing indentation load. An analysis using the selected area electron diffraction pattern (SAEDP) showed that the defects were with streaks along the normal to $\{111\}$ planes. This indicates that they are planar defects, such as stacking faults.

It is very interesting to note that the structure of the material inside the transformation zones changed with indentation load. The analysis of the diffraction pattern (Fig. 4(b)) at the indentation load of 30 and 40 mN shows that the structure in the upper zone is amorphous (Figs. 4 and 5). Under a high resolution mode, it can be seen that the interface between the amorphous phase and the crystalline silicon is not smooth (Fig. 5(c)), containing amorphous pockets and irregularities (Fig. 4(d)). This is consistent with the prediction of molecular dynamic analysis [8]. The anisotropy of the atomic lattice structure of silicon determines the non-smooth transition across the interface. However, the irregular asperities of the indenter surface might also contribute to the formation of the irregular interface.

When the indentation load increases further, to 50 mN say, a new phenomenon appears in the transformation zone. The main part of the material in the zone is still in an amorphous state but a region with non-amorphous structure forms, consisting of small particles of 10–15 nm in diameter (see Fig. 6(b)). This region occupies 5%



(b)

Fig. 6. Subsurface deformation at the indentation load of 50 mN. (a) General view of the damaged zone; (b) the crystalline particles in the transformation zone.

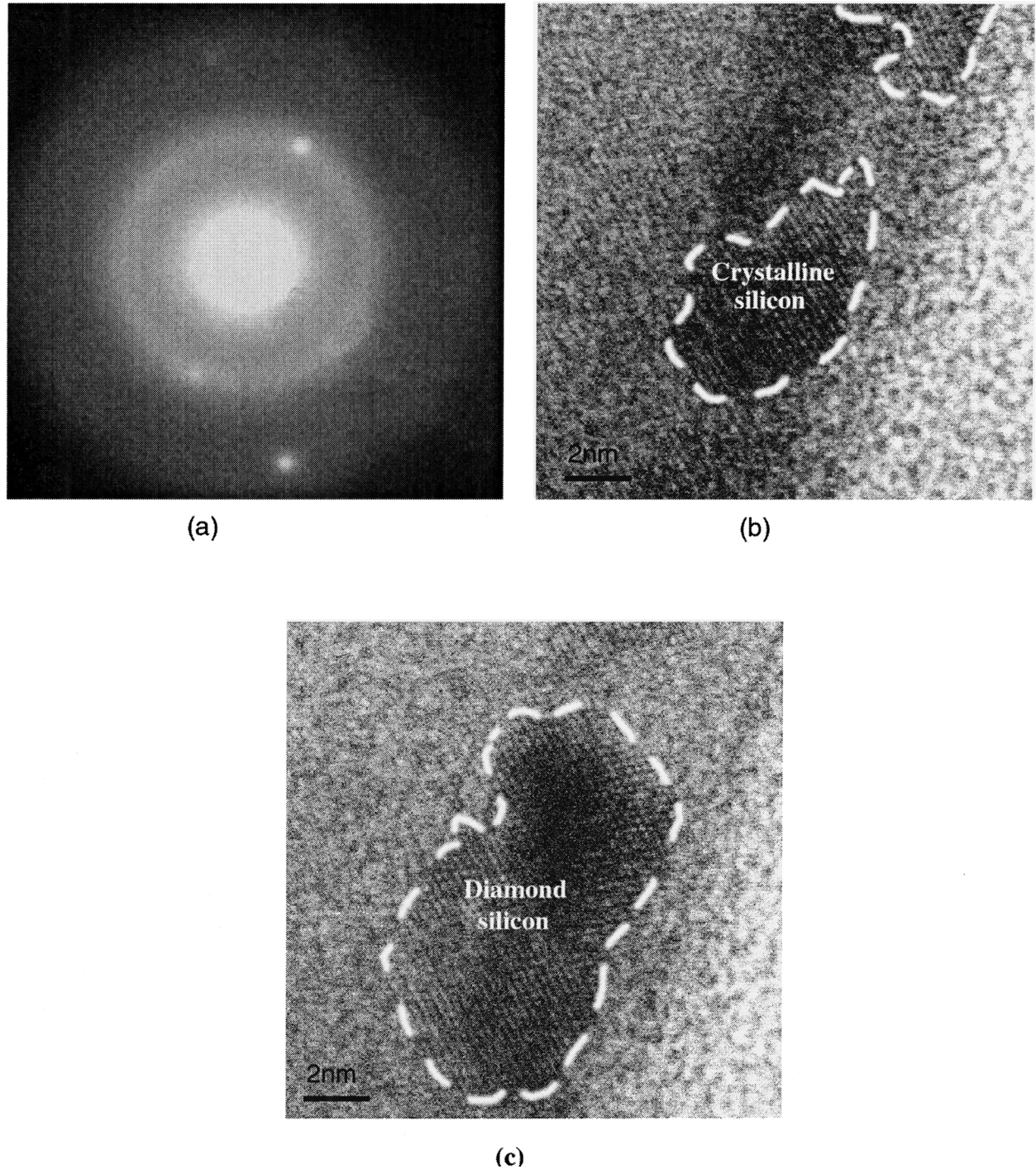


Fig. 7. Details of the transformation zone at the indentation load of 50 mN. (a) The diffraction pattern of the material in the zone; (b) crystalline phase in the amorphous zone; (c) the residual diamond silicon particle in the vicinity of the indented surface due to incomplete amorphous phase transformation.

of the transformation zone and appears in the central part of the zone near its bottom. Although the structure of the particles cannot be identified by the diffraction analysis (Fig. 7(a)) because the size is too small, their crystal nature can be seen clearly under the high-resolution mode (Fig. 7(b)). In addition the high resolution examination also identified some residual crystals of diamond

silicon up to 13 nm in length in the vicinity of the surface (Fig. 7(b)), which were caused by the incomplete phase change during indentation.

With the further increment of indentation load, the above crystal phase inside the amorphous zone grows quickly. At the load of 70 mN, the crystalline phase has occupied about 40% of the whole transformation zone

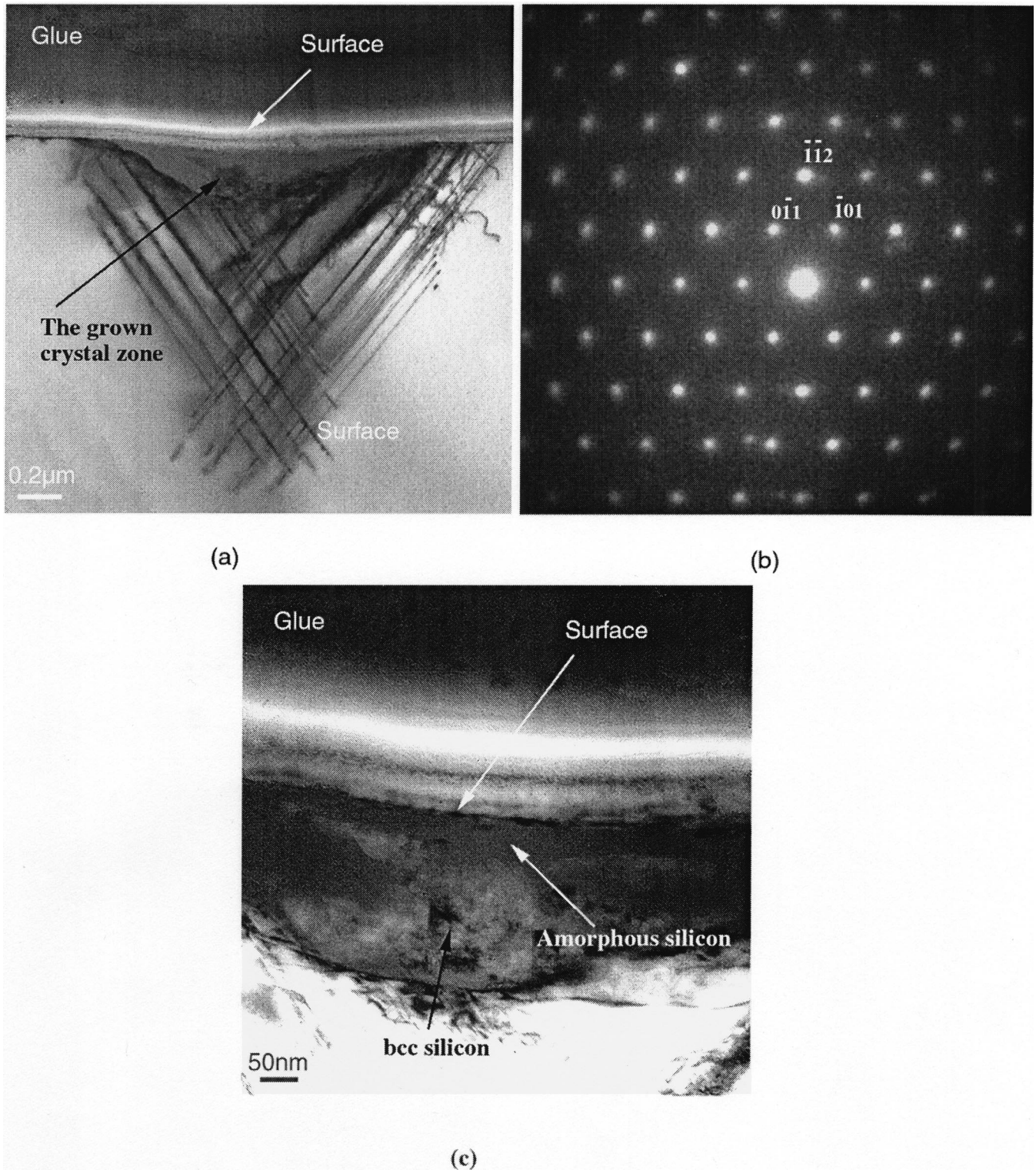


Fig. 8. Subsurface deformation at the indentation load of 70 mN. (a) General view of the damaged zone; (b) diffraction pattern of the material in the transformation zone; (c) bcc silicon particles formed in the amorphous zone.

(see Fig. 8(a)). The crystal structure can now be identified as bcc silicon. The diffraction pattern of the phase with the [111] zone axis can be seen in Fig. 8(b). The crystalline particles in the region have grown to 30–40

nm in diameter, occupy the central part of the transformation zone, but are still surrounded by amorphous silicon (Fig. 8(c)). At this stage, diamond silicon can no longer be detected. This seems to indicate that the increase of

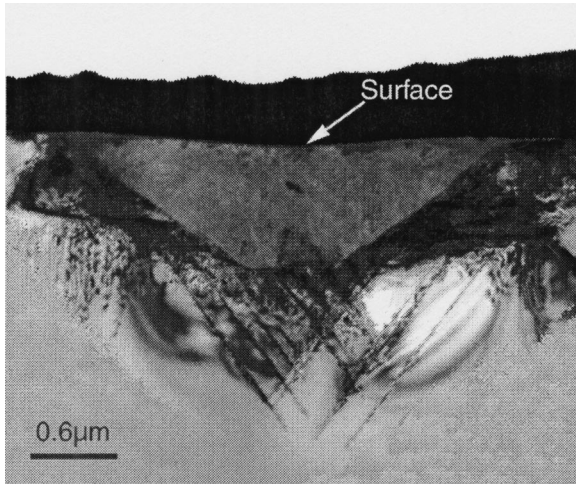


Fig. 9. Subsurface deformation at the indentation load of 90 mN.

the stress level now is sufficient to transform all the diamond silicon into amorphous phase or bcc silicon.

The bcc silicon seems to be stable and grows steadily with the further increase of the indentation load. When the load reaches 90 mN (Fig. 9) the crystalline phase of bcc silicon occupies almost the whole transformation zone, leaving a small amorphous region close to the peripheral edge of the zone. The crystal particles at this stage become 50–60 nm in diameter. Extensive planar defects are emanating from the bottom of the transformation zone.

Some microcracks emerge at the defects intersection when the indentation load increases further. This can be seen more clearly in the subsurface under the indentation load of 100 mN (Fig. 10(a)). The phenomenon is somewhat similar to the cases with glass and zinc sulphide [18,19]. The diffraction pattern (Fig. 10(b)) only indicates a small amount of amorphous phase since it only shows traces of the diffuse amorphous rings. However, the zone axes [111] of the bcc crystals can be distinguished in Fig. 10(b). Crystals of the bcc silicon now become 100 nm in length (Fig. 10(c)–(d)) and cover the whole region of the transformation zone. In addition, crystals of tetragonal silicon also appear in the region. Diffraction pattern with zone axis $[\bar{1}10]$ of the tetragonal silicon can be seen in Fig. 10(b). Fig. 10(e) represents the bright-field image of the crystals of the tetragonal silicon and Fig. 10(f) shows its dark-field image with $g=110$. The appearance of the tetragonal silicon on unloading is direct evidence of the formation of the metallic phase during loading in the indentation of silicon. This is consistent with the theoretical findings by Cheong and Zhang [13].

Now let us analyse the curve corresponding to the penetration of planar defects in the subsurface (Fig. 11). The depth of defect penetration increases sharply until

the load reaches 70 mN. The variation becomes gentle when the load changes from 80 to 90 mN. It then decreases when the load increases further. The phenomenon may be related to the initiation of microcracks at defect intersections. The relaxation with the onset of microcracks may prevent the further penetration of defects in the subsurface.

3.3. The force–displacement behaviour

The force–displacement behaviour of silicon under various indentation loads is shown in Fig. 12. The plastic behaviour is evident even when the load is very small, which is consistent with the observations from Fig. 3(a) as discussed previously. The deviation from the pure elastic curve takes place at an indentation depth of about 20 nm corresponding to an indentation load of 1.3 mN. Hence, non-linear deformation during loading occurs very early, although defects only appear when the indentation load reaches about 30 mN as shown before. Curves during unloading are all characterised by the so-called “pop-out” behaviour. Even at the load of 30 mN two slopes on the unloading path could be located easily. This “pop-out” effect was considered previously as the phase transformation to bcc silicon from the metallic phase during unloading [6]. The present study reveals that the process is more complicated. Phase transformation does take place during unloading for all loads checked, but in the loading range from 30 to 40 mN only amorphous phase transformation takes place. When indentation loads are between 50 and 70 mN, both bcc and amorphous silicon appear up on unloading. However, when indentation load varies from 70 to 100 mN almost all metallic silicon transforms to bcc. Different phases form during unloading depending on the level of loading, while the “pop-out” takes place at all the loading levels. Since both the amorphous and bcc silicon are less dense than metallic silicon, it may be concluded that whenever a phase transformation happens, “pop-out” appears. Furthermore, Fig. 12 seems to indicate that different phase transformation produces different “pop-out” load. The evidence of the difference in phase transformation is clear if we observe the variation of the penetration depth of the indenter at the moment of “pop-out” (Fig. 13). Two slopes exist on the curve. The first corresponds to the load range of 30–50 mN when the amorphous phase transformation dominates during unloading. The second slope covers the load range from 70 to 100 mN when the phase change to bcc silicon becomes the major event during unloading.

By summarising the above investigation we can propose the following scenario for the events in indentation. Under a small indentation load a phase transformation to a metallic phase takes place followed by planar defects under the transformation zone. However, the reverse phase transformation to an amorphous phase

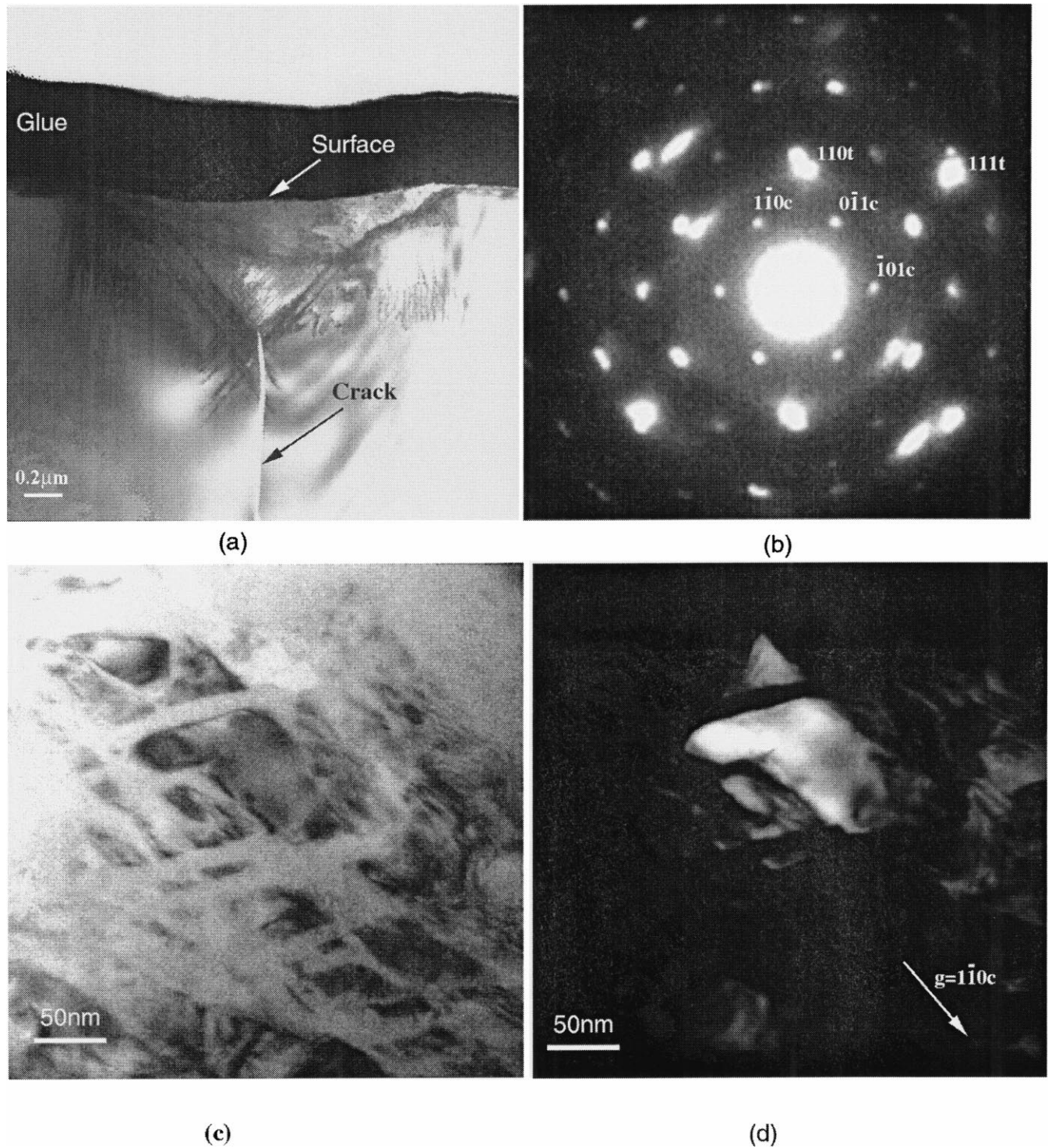
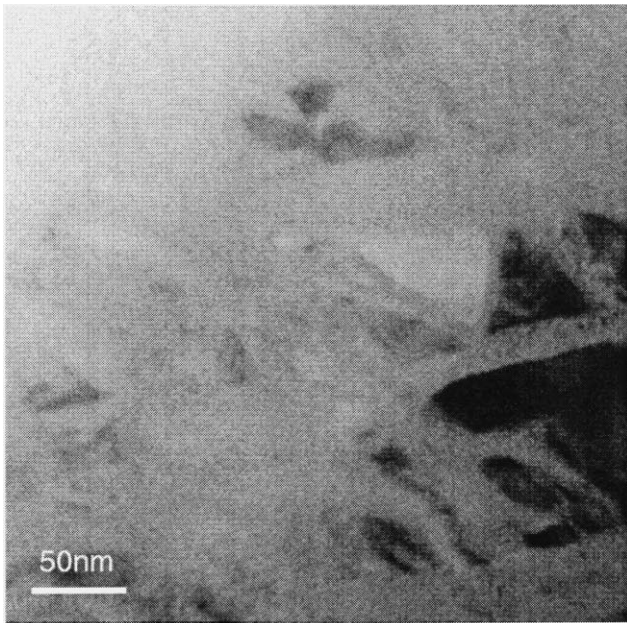


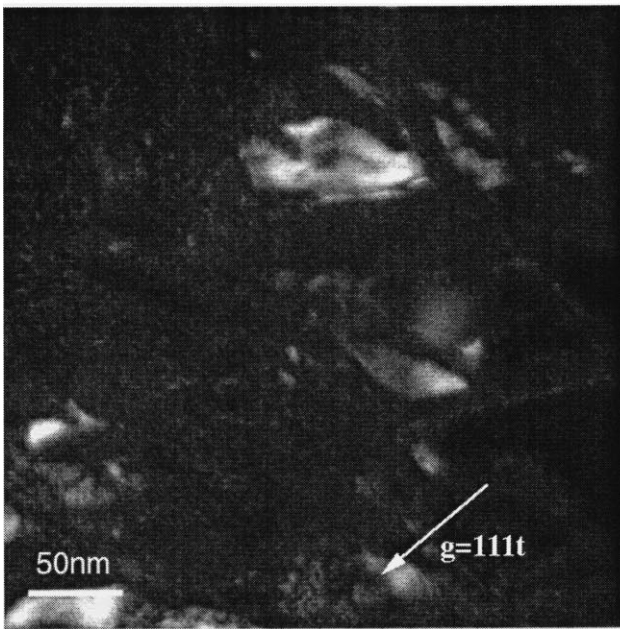
Fig. 10. Subsurface deformation at the indentation load of 100 mN. (a) General view of the damaged zone; (b) diffraction pattern of the material in the transformation zone. Indexed reflections of cubic silicon are notated by “c” and those of the tetragonal silicon are notated by “t”; (c) the bright-field image of the transformation zone; (d) the dark-field image of the same region in the reflection $1\bar{1}0c$; (e) the bright field image of the transformation zone; (f) the dark-field image of the same region in the reflection $111t$.

takes place upon unloading. The increase of the indentation load leads to the formation of bcc silicon during unloading in the middle of the amorphous phase. This phase grows with the increase of indentation load and

finally occupies almost the whole transformation zone. The first microcrack appears at the defects intersection. The interface between the transformation zone and the bulk material is not smooth but contains irregularities



(e)



(f)

Fig. 10. (continued)

and amorphous pockets. The anisotropy of the atomic lattice of silicon is responsible for such phenomenon.

4. Conclusions

Various phase transformations in monocrystalline silicon under indentation were explored for the first time on cross-section view samples. Direct observation with

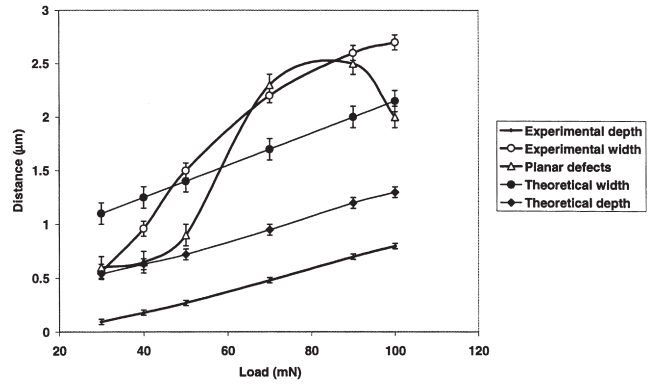


Fig. 11. Experimental and theoretical effect of indentation load on the depth and width of the transformation zone and depth of defect penetration (error bars for theoretical predictions were due to the finite size of spatial steps used in the calculations).

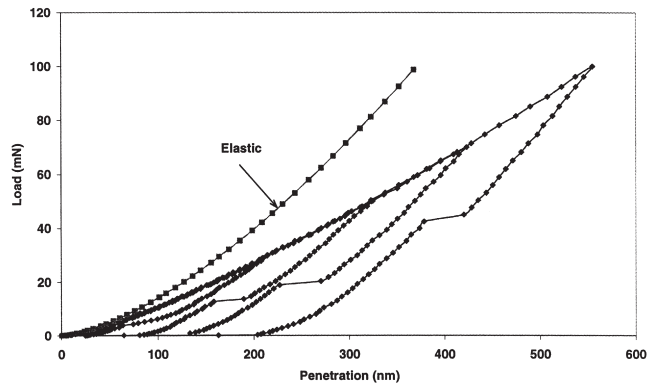


Fig. 12. Force–displacement behaviour at indentation loads of 30, 50, 70 and 100 mN.

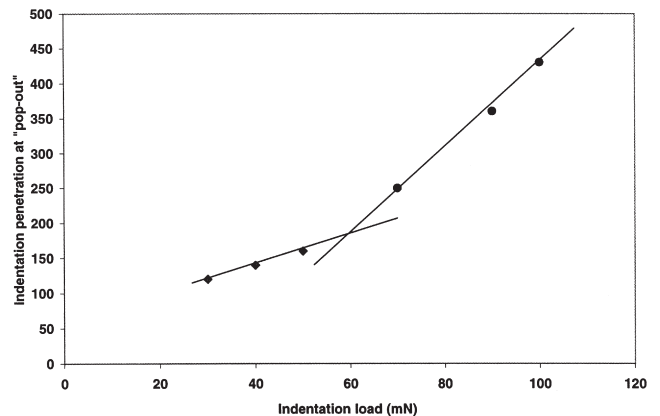


Fig. 13. Effect of the indentation load on the emergence of “pop-out”.

the aid of an electron microscope shows that indentation is accomplished with phase transformation to metallic phase on loading. The reverse phase transformation to amorphous or bcc phases during unloading depends on the maximum indentation load, or in other words, depends on the level of stress field in the plastic zone. Planar defects appear beneath the transformation region.

The purely elastic deformation zone in silicon is very narrow. The “pop-out” phenomenon is related to phase change but different phase change seems to produce different “pop-out” load.

Acknowledgements

The authors wish to thank the Australian Research Council for its continuous support of this project. Thanks are also due to the Electron Microscope Unit of Sydney University for the use of its facilities.

References

- [1] Gridneva V, Milman YUV, Trefilov VI. Phase transformation in diamond-structure crystals during hardness measurements. *Phys Status Solidi (a)* 1972;14:177–82.
- [2] Clarke DR, Kroli MC, Kirchner PD, Cook RF, Hockey BJ. Amorphization and conductivity of silicon and germanium induced by indentation. *Phys Rev Lett* 1988;60:2156–9.
- [3] Parr GM, Oliver WC, Clarke DR. Mechanical behaviour of silicon during small-scale indentation. *J Elect Mater Deform* 1990;19:881–7.
- [4] Parr GM, Oliver WC, Harding DS. New evidence for pressure-induced phase transformation during the indentation of silicon. *J Mater Res* 1991;6:1129–30.
- [5] Field JS, Swain MV. Simple prediction model for spherical indenter. *J Mater Res* 1992;8:297–306.
- [6] Weppelmann ER, Field JS, Swain MV. Observation, analysis, and simulation of the hysteresis of silicon using ultra-micro-indentation with spherical indenters. *J Mater Res* 1993;8:830–40.
- [7] Tanaka H, Zhang LC. Phase transformation of silicon during nano-indentation. In: Zhang LC, Yasunaga N, editors. *Advances in abrasive technology*. Singapore: World Scientific, 1997:43–7.
- [8] Zhang LC, Tanaka H. Nanomechanics in the indentation of monocrystalline silicon. In: *Proceedings of the 2nd Aust. Cong. Appl. Mech.*, 1999, Canberra, pp. 221–226; *JSME Int J Series A: Solid Mech Mater Engng* 1999;42:546–59.
- [9] Zhang LC, Tanaka H. Atomic scale deformation in silicon monocrystals induced by two-body and three-body contact sliding. *Trib Int* 1998;31:425–33.
- [10] Callahan DL, Morris JC. The extent of phase transformation in silicon hardness indentation. *Mater Res* 1992;7:1614–7.
- [11] Page TF, Olive WC, McHargue CJ. The deformation behaviour of ceramic crystals subjected to very low load (nano)indentations. *J Mater Res* 1992;7:450–73.
- [12] Cheong D, Zhang LC. Molecular dynamics simulation of phase transformations in silicon monocrystals to nano-indentation. *Mater Sci Engng A*, in press.
- [13] Cheong D, Zhang LC. Effect of repeated nano-indentations on the deformation in monocrystalline silicon. *J Mater Sci Lett*, in press.
- [14] Zarudi I, Zhang LC. Effect of ultraprecision grinding on the microstructural change in silicon monocrystals. *J Mater Proc Tech* 1998;84:149–58.
- [15] Zarudi I, Zhang LC. Subsurface damage in single-crystal silicon due to grinding and polishing. *J Mater Sci Lett* 1996;15:586–7.
- [16] Bell TJ, Bendeli A, Field JS, Swain MV, Thwait EG. Determination of surface plastic and elastic–plastic properties of ultra micro-indentation. *Metrol* 1991;28:463–9.
- [17] Johnson KL. *Contact mechanics*. Cambridge: Cambridge University Press, 1985.
- [18] Hagan JT. Micromechanics of crack nucleation during indentations. *J Mater Sci* 1979;14:2975–80.
- [19] Van der Zwaag S, Hagan JT, Field JE. Studies of contact damage in polycrystalline zinc sulphide. *J Mater Sci* 1980;15:2965–72.